Sequential-Based Process Modelling of VOCs Photodegradation in Fluidized Beds

Hamid Asadi-Saghandi,[1] Rahmat Sotudeh-Gharebagh,[1]* Amir Motamed Dashliborun,[1] Hossein Kakooei[2] and Mohammad Hajaghazadeh[3]

1. *Process Design and Simulation Research Center, Oil and Gas Centre of Excellence, School of Chemical Engineering, College of Engineering, University of Tehran, P.O. Box 11155-4563, Tehran, Iran*
2. *Occupational Health Department, School of Public Health, Tehran University of Medical Sciences, Tehran, Iran*
3. *Department of Occupational Health, Health Faculty, Urmia University of Medical Sciences, Urmia, Iran*

Sequential modular simulation (SMS), as a new modelling approach, was developed to simulate the photocatalytic oxidation (PCO) of gaseous pollutants in fluidized bed reactors. In the experimental part, the PCO of gaseous acetone was studied in a fluidized bed photo-reactor (FBPR) and the influence of operating conditions (inlet concentration, relative humidity (RH) and superficial gas velocity) on both acetone conversion and mineralization was investigated. It was found that the RH, as a key factor in PCO reactions, had a contradictory effect on the conversion and mineralization of acetone. In the modelling part, the bed was divided into several sections in which the bubble and emulsion phases were considered as a plug flow and a completely mixed flow reactor, respectively. Dynamic two-phase model was adopted as the hydrodynamic sub-model and the Langmuir–Hinshelwood (LH) mechanism as the kinetic sub-model. Kinetic constants of the latter sub-model were estimated using experimental data from the literature. A new dimensionless number (HA number) was introduced to determine the optimum number of sections, as the most important factor in model predictions. The performance of the proposed model was compared with the experimental data obtained in this study and several sets of experimental data from the literature. The results showed that the simple and easy-to-achieve approach, which has the capability of integrating into the industrial process simulators such as Aspen Plus© and Aspen HYSYS©, can be used to simulate the behaviour of non-ideal FBPRs in PCO processes.

Keywords: volatile organic compound (VOC), photodegradation, fluidized bed reactor, TiO_2, sequential modular simulation

INTRODUCTION

The research indicates that growing chemical processes and transportation industries have many undesirable influences on environment and public health. Volatile organic compounds (VOCs), known as a major group of pollutants, are widely emitted from industrial facilities and domestic activities. The extensive usages of VOCs have several environmental and health effects. Both water sources and atmosphere can be easily polluted by them. One of the most adverse effects of VOCs emission is the possibility of dangerous oxidants production such as ozone and peroxyacetyl nitrate. Many of these oxidants are identified to be toxic and some of them are believed to be carcinogenic. Acetone is a typical VOC which is widely used as a solvent in both industrial and domestic applications.[1–5] Therefore, it is vital to find an appropriate method to purify acetone from the air stream.

There are various techniques in order to remove VOCs. Adsorption, condensation, and catalytic combustion are conventional methods that have some drawbacks, such as low removal efficiency and high operating costs. Among removal methods, photocatalytic oxidation (PCO) is a promising technology in which VOCs are oxidized to produce less hazardous products such as CO_2 and H_2O.[2] The PCO process is normally operated at ambient temperature and pressure leading lower energy consumption as compared with conventional processes such as incineration. Moreover, PCO is able to degrade a wide range of pollutants with high decomposition efficiency without further needs to chemical additives. TiO_2 as a common photocatalyst is extensively used in the heterogeneous PCO. This semi-conductor metal oxide is rather inexpensive, chemically stable, and safe, and is also stable against photo corrosion with high photocatalytic activity. These features show its wide usage in purification applications.[6–9] PCO of acetone in air flow using titanium dioxide has previously been studied and the effect of various parameters on its photocatalytic efficiency has been reported.[10–12] The acetone degradation has mainly been investigated in these studies and less attention has been paid to acetone mineralization.

In PCO processes, two general types of reactors are used: fixed and fluidized bed photo-reactors (FBPR). Fluidized bed reactors are preferred due to several advantages. These reactors provide excellent contact between reactant and photocatalyst, superior oxidation rate, higher catalyst loading, close temperature control, and higher mass transfer efficiency. A modified configuration of FBPR as the annulus fluidized bed reactor has been reported by Lim and Kim.[13] This type of reactor not only provides an effective contact among pollutant molecules, catalyst and UV light, but also allows an excellent penetration of UV light into the inner layers.[6–8,13,14] In recent years, various studies have been conducted on PCO technology in which various aspects of this technology have been investigated experimentally. However, less attention has been paid to the modelling and simulation particularly in the case of fluidized beds.[15–17] Recently, Motamed Dashliborun et al.[18] investigated methyl ethyl ketone oxidation in a fluidized bed reactor and

*Author to whom correspondence may be addressed.
E-mail address: sotudeh@ut.ac.ir
Can. J. Chem. Eng. 92:1865–1874, 2014

DOI 10.1002/cjce.22052
Published online in Wiley Online Library (wileyonlinelibrary.com).

compared the obtained experimental data with modelling results using an equation-oriented modelling approach.

In this study, a sequential modular simulation (SMS) approach was developed and validated for an annular FBPR in order to remove acetone from air flow using TiO_2-coated silica gel as the photocatalyst. The relevant calculations began by known feed composition and flow, and continued through the combination of ideal units to obtain all the unknowns in any unit operation in the flowsheet. To simulate the behaviour of a FBPR using SMS approach, several ideal reactors with their well-understood hydrodynamic behaviour and available reaction kinetic models, are linked to each other in the multiphase reactor. This reliable and in-hand method can be used for simulation, optimization, and scale-up of non-ideal FBPRs, so it can facilitate the implementation of non-ideal systems for industrial process simulators.

EXPERIMENTAL

Photocatalyst Preparation and Chemicals

Degussa P-25 (70 % anatase, 30 % rutile; primary particle diameter 30 nm; surface area = 50 m^2/g) was used as the photocatalyst. To improve the fluidization quality of P-25, silica gel (63–200 μm and mean particle diameter of 117 μm) was applied as a substrate. P-25 was coated on transparent silica gel particles by using a simple dip-coating method to prepare TiO_2-coated silica gel (TiO_2/SiO_2).[19] A specific amount of powdered TiO_2 was suspended in distilled water and exposed to ultrasonic waves for 30 min. Afterwards, SiO_2 particles were added and ultrasonication was kept on for another 30 min. The white and homogenous slurry was completely dried overnight at 100 °C. The TiO_2/SiO_2 catalyst was prepared by the calcination of dried slurry at 400 °C for 2 hours. The catalyst loading was 0.2 g P-25 per gram of SiO_2. P-25 was provided from Degussa Corporation (Germany), and the acetone (model pollutant) and SiO_2 were obtained from Merck (Germany).

Fluidized Bed Photo-Reactor (FBPR)

A schematic diagram of annulus fluidized bed reactor is shown in Figure 1 with annulus gap of 7 mm. A 15W UVC lamp with diameter of 26 mm was located in the centre of a cylindrical glass tube with height of 100 cm and inner diameter of 40 mm. A transparent box made of four mica sheets, surrounded the reactor and another four 15W UVA lamps was affixed at the inner walls of the box (not shown in Figure 1). The outer area of the box was wrapped with aluminum foil to minimize the loss of UV light irradiation and to utilize the reflected lights. To uniformly distribute the inlet flow, a sintered glass was installed at the bottom of the glass tube as the gas distributer. The sensor of a thermometer was placed inside the bed to measure its temperature.

The acetone concentration and RH of the inlet air flow were controlled by two bubblers containing acetone and distilled water, respectively. A flow meter (SKC, Inc.) was used to control the flow rate of the inlet stream. The minimum fluidization velocity (U_{mf}) was determined both experimentally and by Wen and Yu correlation.[20] The U_{mf} value was almost 0.8 cm/s in both cases. Experiments were carried out in a wide range of inlet superficial gas velocity (*1*–6 U_{mf}), inlet concentration (300–900 ppm), and RH (15–65 %).

In each experiment, one batch of fresh photocatalyst (37.5 grams) was used to ensure the constant performance of the photocatalyst. No noticeable deactivation was observed under specific operating conditions (conc. = 500ppm, $U/U_{mf} = 2$, RH = 45 %) for almost 40 hours. Approximately, 37.5 g of photocatalyst

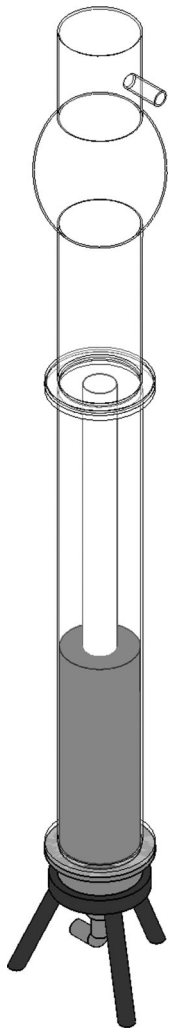

Figure 1. Schematic diagram of the FBPR.

corresponded to 20 cm of bed height. To complete the dark adsorption, the photocatalyst was accommodated in the reactor, and the polluted air flow passed through the reactor without switching lamps on. After the completion of the dark adsorption, the UV lamps were switched on and the PCO process was started. The inlet and outlet gas streams were analyzed using a FID-gas chromatography (Varian CP-3800 instrument equipped with a capillary 50 m × 0.53 mm column). The concentration of CO_2 was measured using a Testo CO_2 analyzer. The obtained results of PCO process were reported under steady state conditions. Most of the experiments were carried out at lower superficial gas velocities to reduce the rate of catalyst attrition and consequently keep constant the reactor performance. Moreover, the disengagement zone at the top of the reactor minimizes the entrainment of the small particles.

PHOTO-REACTOR MODEL

In order to simulate the non-ideal FBPR by combination of ideal reactors, the sequential modular approach was used. As mentioned before, the proposed model is based on dividing the reactor to several sections with equal volumes. Each section consists of two phases and two ideal reactors. The bubble phase (rich in gas) is passed through a plug flow reactor (PFR) and the emulsion phase (rich in solid) is perfectly mixed and passed through a completely

stirred tank reactor (CSTR). In each section, pollutant oxidation takes place in the both reactors and mass transfer occurs just at the exit of reactors between effluent streams. The schematic diagram of this method is shown in Figure 2.

To describe the physical and chemical phenomena occurred in the reactor, two submodels were considered. Hydrodynamic and chemical reaction submodels were coupled together for developing the model and describing these phenomena, respectively. A dynamic two-phase model was adopted as the hydrodynamic submodel and the following assumptions were made to develop the governing equations.[18,21–23]

Radial profiles of the concentration were neglected and eliminated from molar balance equations.

- Steady state conditions were considered for both bubble and emulsion phases in balance equations.
- Due to the low height of the bed, it is assumed that the reactor operates at isothermal conditions. Therefore, physical

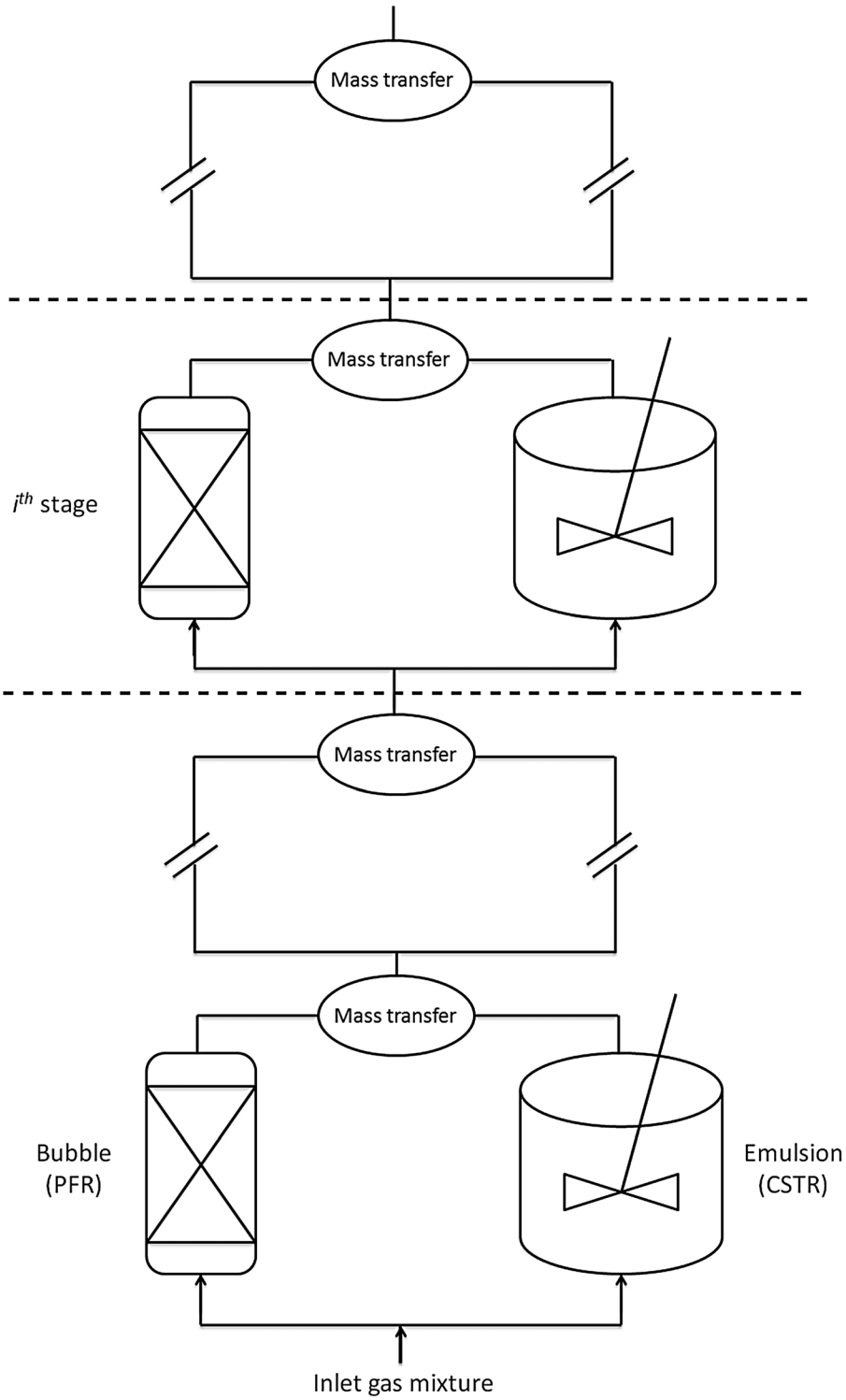

Figure 2. Schematic of sequential modular simulation approach.

properties and hydrodynamic parameters have been considered to be constant.
- Bubble growth is neglected along the bed. It is assumed that the bubbles reach their equilibrium size as soon as they enter the reaction region.

Governing Equations

Based on the aforementioned assumptions, the molar balances in the i^{th} stage for bubble and emulsion phases are as follows:

Bubble phase:

$$C_{Ab(i-1)}U_bA_b - A_b\varepsilon_b\int_{z_{i-1}}^{z_i} r_{A(i)}dz - K_{be}(C_{Ab(i)} - C_{Ae(i)}) \\ V_{b(i)} - C_{Ab(i)}U_bA_b = 0. \quad (1)$$

Emulsion phase:

$$C_{Ae(i-1)}U_eA_e - r_{A(i)}V_{CSTR(i)} + K_{be}(C_{Ab(i)} - C_{Ae(i)}) \\ V_{e(i)}\left(\frac{\delta}{1-\delta}\right) - C_{Ae(i)}U_eA_e = 0. \quad (2)$$

The mass transfer terms (third term in both equations) were calculated in accordance with fluidization and mass transfer equations that are listed in Table 1.[24–27] The volume of the i^{th} stage ($V_{(i)}$), the volume of bubble ($V_{b(i)}$) and emulsion phase ($V_{e(i)}$), and the volume of PFR ($V_{PFR(i)}$) and CSTR ($V_{CSTR(i)}$) in each stage were calculated based on the following equations:

$$V_{(i)} = \frac{V_t}{n}, \quad (3)$$

$$V_{b(i)} = V_{(i)}\delta, \quad (4)$$

$$V_{e(i)} = V_{(i)}(1-\delta), \quad (5)$$

$$V_{PFR(i)} = V_{b(i)}\varepsilon_b, \quad (6)$$

$$V_{CSTR(i)} = V_{e(i)}\varepsilon_e. \quad (7)$$

Afterwards, the calculations are kept on according to the above equations for both phases in all stages until the top of the bed. Required hydrodynamic parameters for Geldart B are presented in Table 2.[20,26,28]

Hydrodynamic Sub-model

There are various hydrodynamic models in the literature to predict the behaviour of fluidized bed hydrodynamics. Among existing models, a dynamic two-phase model (DTP) was chosen to calculate hydrodynamic parameters and characterize properties of bubble and emulsion phases. The existence of solid particle in bubble phase and considering that velocities are higher than minimum fluidization velocity (U_{mf}) for emulsion phase are reasonable assumptions which distinguish this model from other two-phase models.[21,26,29]

Table 2. The required hydrodynamic parameters

Archimedes number	$Ar = \frac{\rho_g d_p^3(\rho_p-\rho_g)g}{\mu_g^2}$
Minimum fluidization velocity	$\frac{U_{mf}\rho_g d_p}{\mu_g} = \sqrt{27.2^2 + 0.0408Ar} - 27.2$
Bubble phase voidage	$\varepsilon_b = 1 - 0.146\exp\left[\frac{-(U-U_{mf})}{4.439}\right]$
Emulsion phase voidage	$\varepsilon_e = \varepsilon_{mf} + 0.2 - 0.059\exp\left[\frac{-(U-U_{mf})}{0.429}\right]$
Bubble phase fraction	$\delta = 0.534 - 0.534\exp\left[\frac{-(U-U_{mf})}{0.413}\right]$

Reaction Sub-model

As reported in the literature, the photocatalytic reaction generally follows the Langmuir-Hinshelwood mechanism. According to this mechanism, the reaction rate has a direct proportion to the surface coverage of pollutant molecule (θ_{VOC}):[30,31]

$$R_{VOC} = k_{\deg}\theta_{VOC} = k_{\deg}\frac{K_{LH}C_{VOC}}{1 + K_{LH}C_{VOC}}, \quad (8)$$

where C_{VOC} is the concentration of VOC, k_{deg} is the intrinsic rate constant, and K_{LH} is the adsorption constant. It should be noticed that there is no general expression that could predict the reaction rate due to the complex mechanism of reactions. Some simplifications have been adopted in Equation (8); for example, the possible interference of intermediates and by-products has been neglected in Equation (8).[15,16,31,32]

Rate law parameters were determined applying a nonlinear optimization program. σ^2 was minimized to estimate the kinetic constants of L-H model:[18]

$$\sigma^2 = \sum_{i=1}^{N}\frac{(R_{VOC\exp,i} - R_{VOCc,i})^2}{N-K}, \quad (9)$$

where N is the total number of experiments, K is the number of parameters that should be determined ($K=2$ in this study), $R_{VOCc,i}$ is the calculated reaction rate for experiment i, and $R_{VOCexp,i}$ is the experimental reaction rate for experiment i, which is defined as follows:

$$R_{VOC\exp} = \frac{Q(C_{VOC,in} - C_{VOC,out})}{W}, \quad (10)$$

Table 1. Fluidization and mass transfer correlations

Bubble diameter	$D_b = 0.21H^{0.8}(U-U_{mf})^{0.42}\exp[-0.25(U-U_{mf})^2 - 0.1(U-U_{mf})]$
Bubble velocity	$U_b = U - U_e + u_{br}$
Bubble rise velocity	$u_{br} = 0.711\sqrt{gD_b}$
Emulsion velocity	$U_e = \frac{U-\delta U_b}{1-\delta}$
Bubble-to-emulsion mass transfer coefficient	$\frac{1}{K_{be}} = \frac{1}{K_{bc}} + \frac{1}{K_{ce}}$
	$K_{bc} = 4.5\left(\frac{U_e}{D_b}\right) + 5.85\left(\frac{D_{AB}^{1/2}g^{1/4}}{D_b^{5/4}}\right)$
	$K_{ce} = 6.77\left(\frac{D_{AB}\varepsilon_e u_{br}}{D_b^3}\right)^{1/2}$

in which Q is the total flow rate of inlet gas, $C_{VOC,in}$ is the concentration of VOC at the inlet, $C_{VOC,out}$ is the concentration of VOC at the outlet of the reactor, and W is the weight of photocatalyst in the reactor.

RESULTS AND DISCUSSION

The PCO efficiency of VOCs removal has widely been investigated in the literature by considering the photocatalytic conversion of VOCs.[6–8,33–38] Less attention has been paid to mineralization, particularly in FBPRs. In fact, mineralization is the main index of PCO process expressing less hazardous productions, such as CO_2 and H_2O. Therefore, it is essential to compare both conversion and mineralization to study the efficiency of PCO reactions. In this study, the conversion of acetone was calculated from the difference between the inlet and outlet acetone concentrations, and the mineralization was determined using the following equation:

$$mineralization = \frac{[CO_2]_{out}}{\alpha[acetone]_{in}}, \quad (11)$$

where α is the number of carbon atoms in the molecule of model pollutant ($\alpha = 3$ for acetone).

One of the important factors that can largely influence the PCO performance is RH. Many researchers have studied RH effect on acetone removal and presented different or sometimes inconsistent results due to the very complex effect of this factor on photocatalytic degradation.[10,11,39–44] For example, wet conditions could improve the conversion by degrading the inlet VOC molecules but have the inhibiting effect on CO_2 production. Experiment operating conditions, such as initial concentration and temperature, the nature of VOC molecule, specific characteristics of photocatalyst, oxygen partial pressure, and the presence of impurities, are some of the agents that can be a determinant in RH effects on VOC removal.[39,44–46]

Generally, there are two explanations in the literature that justify the positive or negative effect of RH on degradation or mineralization of VOCs.[47] In the case of conversion, the degradation progress is attributed to OH radicals where more are produced in wet conditions. Competitive adsorption between H_2O and VOC molecules is considered as an adverse factor that can aggravate the removal conversion. In the case of mineralization, wet conditions can improve the degradation of intermediate products towards CO_2 and H_2O owing to more production of OH radicals. The presence of water molecules can hinder the mineralization due to the competitive adsorption between the intermediates and H_2O molecules and, consequently, hamper desorption of the intermediates from the TiO_2 surface.[48]

Figure 3 shows the influence of RH on acetone (here and in Choi et al.),[49] methyl ethyl ketone (MEK),[33] trichloroethylene (TCE),[50] and formaldehyde (HCHO)[51] conversions. As illustrated in Figure 3, the RH has a negative effect on the VOCs conversion in the whole range of RH. This means that in these cases, the competitive adsorption is a dominant factor and high concentration of OH radicals does not improve the VOCs conversion. This figure also reveals that the RH effect on the VOCs degradation is highly dependent on the nature of reactants. As can be seen, RH has the greatest impact on the formaldehyde conversion, whereas the conversion of TCE is not significantly affected by RH. The opposing role of water on acetone degradation has already been reported in the literature.[11,39–41]

Figure 4 illustrates the influence of RH on acetone (this study) and methyl isobutyl ketone (MIBK) mineralization.[44] The mean

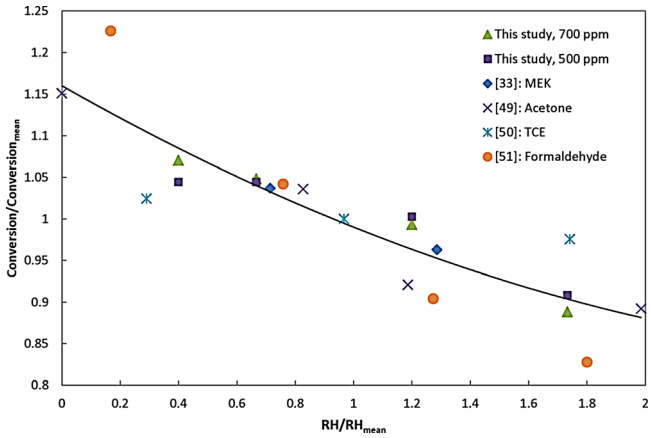

Figure 3. Influence of RH on acetone, MEK, TCE and formaldehyde conversion.

values of conversion, mineralization and RH are shown in Table 3. According to Figure 4, there is an optimum RH in the case of acetone mineralization. Similar result was reported by Coronado et al.[44] for MIBK mineralization in which the maximum mineralization was obtained at moderate RH. The mineralization of acetone improves up to 45 % of RH (Mineralization/Mineralization$_{mean} = 1.2$), and afterwards a further increase in RH will decrease the yield of CO_2. Since mineralization is the final step of PCO reactions, the intermediates have a crucial role in CO_2 production.

Acetate, formate, formic acid, and acetaldehyde have been reported in the literature as the intermediates for acetone photodegradation.[39] The mentioned effect of RH on CO_2 yield could be explained as follows: at RH of $\leq$45 %, OH radicals improve the mineralization through the decomposition of intermediates towards CO_2, but with the further increase in RH, competitive adsorption between the intermediates and water molecules aggravates the CO_2 yield. Comparison of the conversion and mineralization values indicates that the carbon balance is not established for acetone degradation, so intermediates production is likely. However, more experiments should be carried out to identify the intermediates and the effect of RH on their decomposition. In addition, it can be deduced from Figure 4 that with increasing the initial concentration, the CO_2 yield decreases. This is attributed to the fact that at higher coverage of initial concentration, more intermediates are produced. Also, the increase

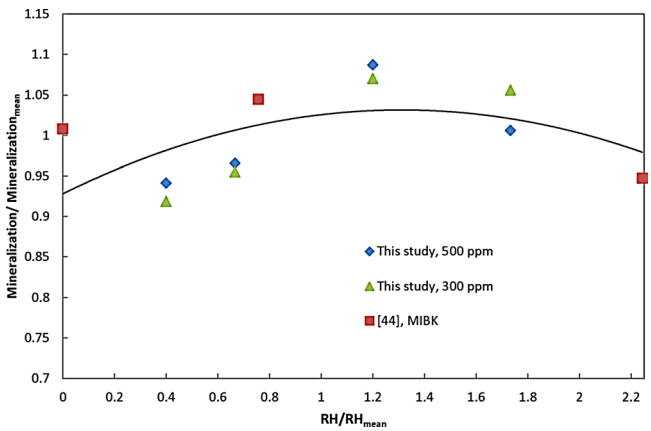

Figure 4. Influence of RH on acetone and MIBK mineralization.

Table 3. The mean values of conversion, mineralization and RH

Experiment set	RH_{mean}	$Conv._{mean}$	$Min._{mean}$
This study, 700 ppm	37.5	90.63	—
This study, 500 ppm	37.5	95.75	—
[33]	35	94.5	—
[49]	1.81	17.38	—
[50]	51.67	82	—
[51]	32.3	65.25	—
This study, 500 ppm	37.5	—	61.63
This study, 300 ppm	37.5	—	69.13
[44]	37	—	82.3

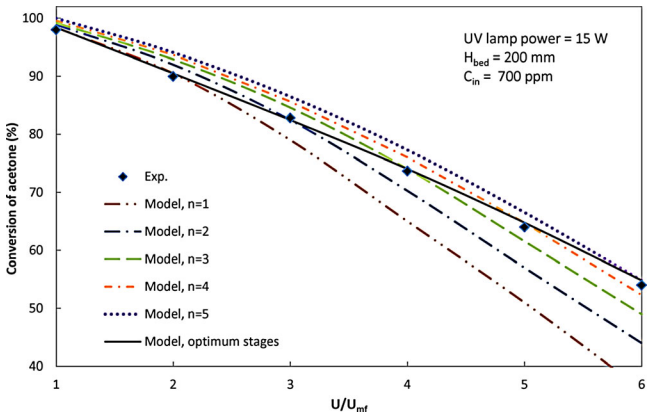

Figure 5. Experimental and simulation results of acetone conversion as a function of superficial gas velocity (RH = 45 %) at different number of stages and optimum number of stages, the values of "HA" for the experimental data (U/Umf = 1–6) are 56.36, 23.7, 20.01, 13.52, 9.98, and 7.82, respectively.

in concentration may change the reaction path towards other intermediates instead of CO_2.[6,8]

The kinetic parameters of L-H mechanism are listed in Table 4. The kinetic parameter values in the study of Motamed Dashliborun et al.[18] were used for toluene, trichloroethylene (TCE), and methyl ethyl ketone (MEK), and calculations were performed for acetone in RH of 25 and 45 %. To evaluate the results from a quantitative point of view, correlation coefficient (CC) was determined based on the following equation:

$$CC = \frac{\sum_{i=1}^{N}(X_i - \bar{X})(Y_i - \bar{Y})}{\sqrt{\sum_{i=1}^{N}(X_i - \bar{X})^2 \sum_{i=1}^{N}(Y_i - \bar{Y})^2}}, \quad (12)$$

where X_i and Y_i represent the experimental and calculated values, respectively, and N is the total number of observations. $\bar{X}$ and $\bar{Y}$ are the mean values of experimental and predicted data, respectively.

The acetone conversion against superficial gas velocity and the model predictions are presented in Figure 5. As is shown in this figure, the superficial gas velocity has a significant effect on acetone conversion, and acetone conversion dropped dramatically with increasing the inlet flow rate. At higher flow rates, the volume of bubble phase increases, which leads to a shorter residence time and decreasing the acetone conversion.[6,52] In addition, Figure 5 illustrates that the number of stages (n) is a crucial parameter in model validity. Also, this figure shows the model predictions at an optimum number of stages. Therefore, it is important to find a procedure to estimate the optimum number of stages in order to predict the experimental results properly.

A newly defined dimensionless number (HA) is introduced to find the optimum number of stages. There are several parameters influencing on the number of stages. The parameters that had the most effect were classified in three categories: hydrodynamic, reaction, and UV. Superficial gas velocity, minimum fluidization velocity, photocatalyst particle size, difference between gas and solid density (in the frame work of Ar number), and aspect ratio (height of reactor over reactor diameter) were the most important hydrodynamic parameters affecting the number of stages. Kinetic constants and UV light intensity were considered in the reaction and UV categories, respectively. Several sets of experimental data were used to find the effect of these parameters on HA number that presented in Table 5.

In the hydrodynamic side, increasing the Archimedes number (i.e., the higher ρ_g-ρ_s) has an adverse effect on fluidization quality due to the inability of particles to fluidize readily. Uniform distribution of UV light is a very important factor on PCO reactions. So the higher the Archimedes number, the lower the degradation efficiency obtained. A similar conclusion is established for the higher particle size of the photocatalyst. In addition, by increasing of the superficial gas velocity, the residence time is decreased that allows the bypass of reactant molecules without participating in the reaction and consequently the decrease of the conversion.

In the matters of reaction kinetic and lamp properties, a slower reaction or a UV lamp with lower light intensity has a negative effect on removal of VOC. Therefore, the number of stages should be increased to reach a particular photodegradation conversion. Based on the sets of experimental data shown in Table 5, a new dimensionless number was proposed to determine the optimum number of stages in PCO processes as

$$HA = 10^5 \left(\frac{I}{I_{\max}}\right)^{0.55} \left(K_{LH}\frac{k_{\deg}\rho_b}{K_{be}}\right)^{0.1} \left(\frac{Re_{\mathrm{mf}}}{Re\,Ar}\right)^{1.25} \gamma^{-1}, \quad (13)$$

in which I_{max} is the maximum UV light intensity above which the rate of PCO reaction would not increase, Re_{mf} is the particle Reynolds number at minimum fluidization velocity, γ denotes the aspect ratio of reactor, ρ_b is the bulk density of bed, and K_{be} is the bubble to emulsion mass transfer coefficient. The number of the stages as a function of the HA dimensionless number are shown in Table 6.

The parity plot of calculated versus experimental conversion is presented in Figure 6. The figure shows that the predicted results of model are in a close agreement with experimental data, moreover the model predictions were evaluated quantitatively using errors statistics indicators such as BIAS and Scatter Index (SI), which are

Table 4. Kinetic parameters of Langmuir-Hinshelwood model

Compounds	k_{deg} (μmol/g s)	K_{LH} (Lit/μmol)	CC
Acetone (RH = 25 %)	1.29	0.0025	0.98
Acetone (RH = 45 %)	3.43	0.0011	0.99
MEK (RH = 25 %)	0.750	0.0044	0.99
MEK (RH=45 %)	0.203	0.0177	0.97
TCE	13.23	0.1538	0.93
Toluene	0.183	4.367	0.95

Table 5. The experimental operating conditions

Characteristic	Unit	This study	[18]	[13]	[6]	[34]	[35]
Pollutant	—	Acetone	MEK	TCE	TCE	TCE	Toluene
H	mm	200	100	220	220	100	135
D_i	mm	26	26	39	39	60	39
D_o	mm	40	40	55	55	70–90	49
Lump UV	W	15	15	10	10	15	15
d_p	μm	62–200	74–250	250–590	250–590	250–417	125–425
ρ_s	kg/m^3	2110	3246	2190	2190	2200	1400
C	ppm	300–900	100–800	212	100–500	20–230	5–32
T	°C	30	30	30	30	30	30
P	kPa	101	101	101	101	101	101
U_{mf}	cm/s	0.804	1.17	1.7	1.7	4.9	1.06–1.23
U	cm/s	U_{mf}-6U_{mf}	U_{mf}-4U_{mf}	U_{mf}-6U_{mf}	3U_{mf}	0.5U_{mf}-4U_{mf}	1–6
Geldart	—	B	B	B	B	B	B

Table 6. Number of stages defined by "HA" dimensionless number

Range	n
$23.5 \leq HA$	1
$17.3 \leq HA < 23.5$	2
$12 \leq HA < 17.3$	3
$8.2 \leq HA < 12$	4
$HA < 8.2$	5

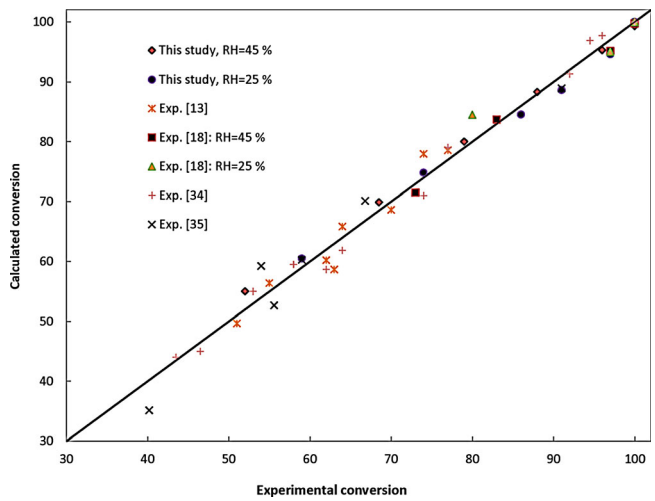

Figure 6. Comparison of experimental and simulation results in terms of conversion.

Table 7. BIAS and SI of model results for different experiments

Reactor results	*BIAS*	*SI*
This study	0.048	0.017
[6]	−0.18	0.037
[13]	0.015	0.038
[18]	0.061	0.021
[34]	0.054	0.026
[35]	0.037	0.059

defined by the following equations:

$$BIAS = \sum_{i=1}^{N} \frac{1}{N}(Y_i - X_i), \tag{14}$$

$$SI = \frac{\sqrt{(1/N)\sum_{i=1}^{N}(Y_i - X_i)^2}}{\bar{X}_i}. \tag{15}$$

X_i, Y_i, $\bar{X}$, and $\bar{Y}$ were represented before. The small amount of error results, which are presented in Table 7, show the validity of this model from the statistics point of view.

Figures 7, 8, and 9 show the influence of initial concentration on the removal of acetone, TCE, and toluene, respectively. As can be seen in these figures, the conversion of VOC decreases by increasing the initial concentration. In the lower amounts of initial concentration, the degradation efficiency is 100 %. Further increase in initial concentration will decrease the conversion. In the lower initial concentration, the numbers of active sites are enough to degrade the inlet pollutant molecules. But since the numbers of active sites on the surface of TiO_2 are limited, further increase in inlet concentration will decrease the photodegradation conversion. Furthermore, increasing the initial concentration can enhance the production of intermediates which occupy the active sites.[6,13,35]

Figure 7 also illustrates the influence of RH on the conversion of acetone in two levels of RH. In general, the conversion of acetone in 25 % RH is higher than in 45 % RH. The initial concentration of acetone is also an important factor. At the low level of the initial concentration (300 ppm), the increase of RH does not decrease the degradation of acetone. It might be indicated that there are sufficient amounts of active sites on the surface of photocatalyst at this level of the initial concentration. Further increase in the initial concentration leads to a competitive adsorption between the water and acetone molecules and consequently the evidence of RH effect on the acetone conversion.

These figures also illustrate that the model predictions are in a close agreement with experiment data of acetone, toluene, and TCE degradation. The slight deviation could be attributed to the fact that the constants of hydrodynamic parameters were calculated by Cui et al.[28] for a particle (Geldart B) which is not exactly the same as the particles employed in these cases. Therefore, a little deviation was observed for the degradation of acetone, toluene, and TCE.[21]

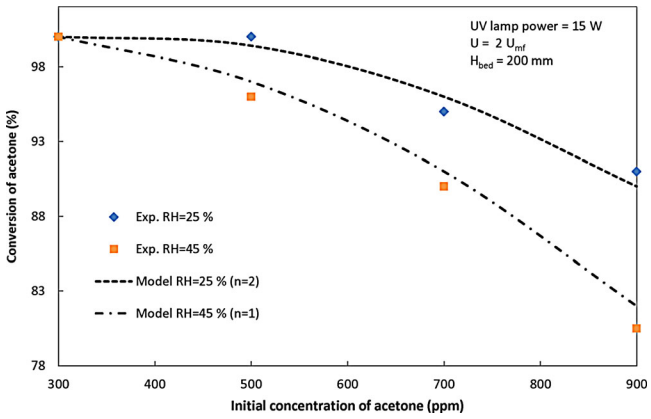

Figure 7. Experimental and simulation results of acetone conversion as a function of initial concentration at two different RH.

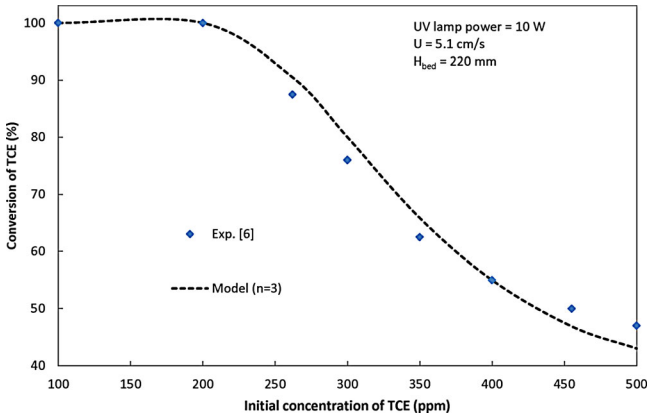

Figure 8. Experimental and simulation results of TCE conversion as a function of initial concentration.

The optimum number of stages in model predictions are also shown in the figures.

The effect of bed height on the conversion of toluene is depicted in Figure 10. As can be seen in this figure, the decomposition of toluene improves by increasing the bed height. In fact, the amount of catalyst that is used in the reactor will increase with the increase in bed height, so the number of active sites which can take part in

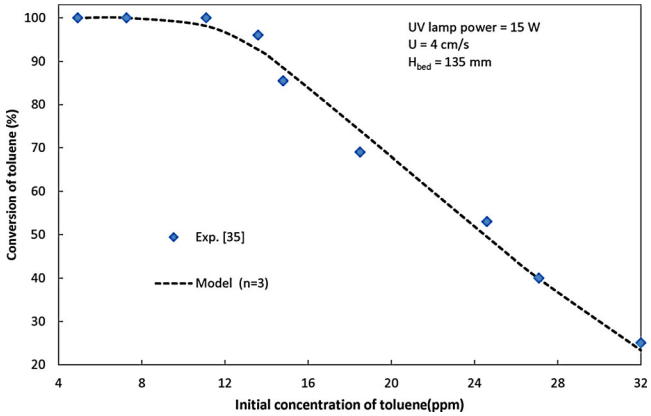

Figure 9. Experimental and simulation results of toluene conversion as a function of initial concentration.

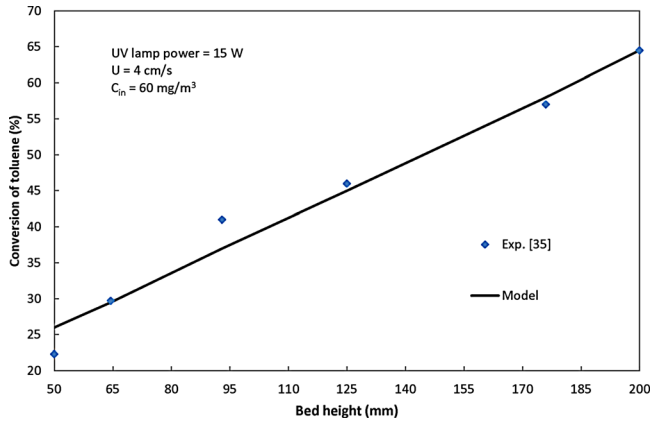

Figure 10. Comparison of experimental and simulation results of toluene conversion at different bed heights.

the reaction increases. Also, the residence time increases with increasing the bed height that improves the efficiency of removal.[35] Furthermore, Figure 10 shows that the variation of the conversion is almost linear as a function of the bed height which is in good agreement with model predictions.

CONCLUSION

The acetone degradation was studied in a fluidized bed reactor of TiO_2/SiO_2 particles. The effect of operating conditions was investigated on both conversion and mineralization of acetone. The results show that the RH has an opposing effect on acetone conversion in the whole range of RH (15–65 %). However, the mineralization will be improved with increasing the relative humidity up to 45 % of RH. Sequential modular approach was developed to simulate PCO processes in FBPRs. A new dimensionless number (HA) was introduced to estimate the optimum number of stages as the most important part of the model. Satisfactory results of model in prediction of the experimental data illustrate that the model can be employed in simulation of the non-ideal fluidized bed photo-reactors.

NOMENCLATURE

A	cross-sectional area (m^2)
Ar	Archimedes number ($d_p^3\rho_g(\rho_s-\rho_g)g/\mu_g^2$)
$BIAS$	bias of data
C_A	concentration of component A (mol/m^3)
CC	correlation coefficient
D_{AB}	diffusion coefficient (m^2/s)
D_b	bubble mean diameter (m)
D_i	inner diameter of reactor (m)
D_o	outer diameter of reactor (m)
d_p	particle diameter (m)
g	acceleration of gravity (m/s^2)
H	bed height (m)
HA	proposed dimensionless number
I	UV light intensity (w/m^2)
K_{bc}	bubble to cloud mass transfer coefficient (1/s)
K_{be}	bubble to emulsion mass transfercoefficient(1/s)
K_{ce}	cloud to emulsion mass transfer coefficient (1/s)
K_{LH}	adsorption constant (m^3/mol)
k_{deg}	rate constant (mol/kg.s)
n	number of stages

N number of observations
P reactor operating pressure (kpa)
Q total flow rate (m^3/s)
R reaction rate (mol/kg.s)
r_A reaction rate based on component A (mol/m^3.s)
Re particle Reynolds number
T reactor operating temperature (K)
U superficial gas velocity (m/s)
U_b bubble velocity (m/s)
U_e emulsion velocity (m/s)
U_{mf} minimum fluidization velocity (m/s)
V_b bubble phase volume (m^3)
V_e emulsion-phase volume (m^3)
W weight of photocatalyst (kg)
z distance from distributor (m)

Greek letters

δ bubble phase fraction
θ surface coverage
γ aspect ratio
ρ_g gas density (kg/m^3)
ρ_s solid density (kg/m^3)
ρ_b bulk density (kg/m^3)
μ_g gas viscosity (Pa.s)
ε average bed porosity
ε_b bubble phase porosity
ε_e emulsion phase porosity

Subscripts

b bubble
e emulsion
in inlet
mf evaluated at minimum fluidizing velocity
out outlet

ACKNOWLEDGMENTS

The authors would like to thank the Iran Nanotechnology Initiative Council and the Iran National Science Foundation (INSF-Grant no. G011) for their valuable support.

REFERENCES

[1] S. M. Japar, T. J. Wallington, S. J. Rudy, T. Y. Chang, *Environ. Sci. Technol.* **1991**, *25*, 415.

[2] R. M. Alberici, W. F. Jardim, *Appl. Catal., B* **1997**, *14*, 55.

[3] T. M. Sack, D. H. Steele, K. Hammerstrom, J. Remmers, *Atmos. Environ., Part A* **1992**, *26*, 1063.

[4] K. Wolf, A. Yazdani, P. Yates, *J. Air Waste Manage. Assoc.* **1991**, *41*, 1055.

[5] P. Monneyron, M. H. Manero, S. Manero, *Can. J. Chem. Eng.* **2007**, *85*, 326.

[6] T. H. Lim, S. D. Kim, *Chemosphere* **2004**, *54*, 305.

[7] O. Prieto, J. Fermoso, R. Irusta, *Int. J. Photoen.* **2007**, *2007*, 1.

[8] Q. Geng, Q. Guo, X. Yue, *Ind. Eng. Chem. Res.* **2010**, *49*, 4644.

[9] P. Pichat, J. M. Herrmann, H. Courbon, J. Disdier, M. N. Mozzanega, *Can. J. Chem. Eng.* **1982**, *60*, 27.

[10] G. B. Raupp, C. T. Junio, *Appl. Surf. Sci.* **1993**, *72*, 321.

[11] J. Peral, D. F. Ollis, *J. Catal.* **1992**, *136*, 554.

[12] M. E. Zorn, D. T. Tompkins, W. A. Zeltner, M. A. Anderson, *Appl. Catal., B* **1999**, *23*, 1.

[13] T. H. Lim, S. D. Kim, *Korean J. Chem. Eng.* **2002**, *19*, 1072.

[14] A. Brucato, D. Iatridis, P. Yue, L. Rizzuti, *Can. J. Chem. Eng.* **1992**, *70*, 1063.

[15] A. O. Ibhadon, I. M. Arabatzis, P. Falaras, D. Tsoukleris, *Chem. Eng. J.* **2007**, *133*, 317.

[16] V. Tomašić, F. Jović, Z. Gomzi, *Catal. Today* **2008**, *137*, 350.

[17] Y. Boyjoo, M. Ang, V. Pareek, *Chem. Eng. Sci.* **2013**, *93*, 11.

[18] A. Motamed, R. Dashliborun, M. Sotudeh-Gharebagh, H. Hajaghazadeh, S. Kakooei, *Afshar, Chem. Eng. J.* **2013**, *226*, 59.

[19] T. H. Lim, S. D. Kim, *Korean J. Chem. Eng.* **2004**, *21*, 905.

[20] C. Wen, Y. Yu, *AlChE J.* **1966**, *12*, 610.

[21] R. Jafari, R. Sotudeh-Gharebagh, N. Mostoufi, *Chem. Eng. Technol.* **2004**, *27*, 123.

[22] A. Hashemi Sohi, A. Eslami, A. Sheikhi, R. Sotudeh-Gharebagh, *Energy Fuels* **2012**, *26*, 2058.

[23] A. Sheikhi, R. Sotudeh-Gharebagh, A. Eslami, A. H. Sohi, *Biochem. Eng. J.* **2012**, *63*, 95.

[24] P. Cai, M. Schiavetti, G. De Michele, G. Grazzini, M. Miccio, *Powder Technol.* **1994**, *80*, 99.

[25] D. Kunii, O. Levenspiel, *Fluidization Engineering*, 2nd edition, Butterworth-Heineman, Boston **1991**.

[26] N. Mostoufi, H. Cui, J. Chaouki, *Ind. Eng. Chem. Res.* **2001**, *40*, 5526.

[27] S. Sanaei, N. Mostoufi, R. Radmanesh, R. Sotudeh-Gharebagh, C. Guy, J. Chaouki, *Can. J. Chem. Eng.* **2010**, *88*, 1.

[28] H. Cui, N. Mostoufi, J. Chaouki, *Chem. Eng. J.* **2000**, *79*, 133.

[29] J. Chaouki, A. Gonzalez, C. Guy, D. Klvana, *Chem. Eng. Sci.* **1999**, *54*, 2039.

[30] T. N. Obee, R. T. Brown, *Environ. Sci. Technol.* **1995**, *29*, 1223.

[31] G. Vincent, A. Queffeulou, P. M. Marquaire, O. Zahraa, *J. Photochem. Photobiol. A* **2007**, *191*, 42.

[32] A. Bouzaza, A. Laplanche, *J. Photochem. Photobiol. A* **2002**, *150*, 207.

[33] M. Hajaghazadeh, H. Kakooei, A. M. Dashliborun, R. Sotudeh-Gharebagh, F. Golbabaie, S. Afshar, A. R. Foroushani, *Fresenius Environ. Bull.* **2013**, *22*, 435.

[34] S. K. Lee, J. S. Kim, I. K. Kim, J. K. Lee, *Stud. Surf. Sci. Catal.* **2006**, *159*, 581.

[35] X. Zhang, C. Liao, "Photocatalytic Degradation of Toluene by Nano-TiO_2 in a Fluidized Bed," *The 12th International Conference on Fluidization – New Horizons in Fluidization Engineering*, F. Berruti, X. Bi, T. Pugsley, Eds., ECI Symposium Series, Volume RP4, 13–17 May, **2007**.

[36] M. Hajaghazadeh, H. Kakooei, A. M. Dashliborun, R. Sotudeh-Gharebagh, F. Golbabaie, A. R. Foroushani, S. Afshar, *Fresenius Environ. Bull.* **2013**, *22*, 1719.

[37] G. Vincent, P. M. Marquaire, O. Zahraa, *J. Photochem. Photobiol. A* **2008**, *197*, 177.

[38] M. Hajaghazadeh, V. Vaiano, D. Sannino, H. Kakooei, R. Sotudeh-Gharebagh, P. Ciambelli, *Catal. Today* **2013**, *230*, 79.

[39] M. A. Henderson, *J. Catal.* **2008**, *256*, 287.

[40] C. Raillard, V. Hequet, P. Le Cloirec, J. Legrand, *J. Photochem. Photobiol. A* **2004**, *163*, 425.

[41] M. L. Sauer, D. F. Ollis, *J. Catal.* **1994**, *149*, 81.

[42] D. Kozlov, A. Panchenko, D. Bavykin, E. Savinov, P. Smirniotis, *Russ. Chem. Bull.* **2003**, *52*, 1100.

[43] Y. Ku, K.-Y. Tseng, W.-Y. Wang, *Water, Air, Soil Pollut.* **2005**, *168*, 313.

[44] J. M. Coronado, M. E. Zorn, I. Tejedor-Tejedor, M. A. Anderson, *Appl. Catal., B* **2003**, *43*, 329.

[45] C. Raillard, V. Héquet, P. L. Cloirec, J. Legrand, *Appl. Catal., B* **2005**, *59*, 213.

[46] S. B. Kim, H. T. Hwang, S. C. Hong, *Chemosphere* **2002**, *48*, 437.

[47] O. Debono, F. Thévenet, P. Gravejat, V. Héquet, C. Raillard, L. Le Coq, N. Locoge, *J. Photochem. Photobiol. A* **2013**, *258*, 17.

[48] T. M. Twesme, D. T. Tompkins, M. A. Anderson, T. W. Root, *Appl. Catal., B* **2006**, *64*, 153.

[49] W. Choi, J. Y. Ko, H. Park, J. S. Chung, *Appl. Catal., B* **2001**, *31*, 209.

[50] W.-K. Jo, K.-H. Park, *Chemosphere* **2004**, *57*, 555.

[51] C. Ao, S. Lee, J. Yu, J. Xu, *Appl. Catal., B* **2004**, *54*, 41.

[52] T. H. Lim, S. M. Jeong, S. D. Kim, J. Gyenis, *J. Photochem. Photobiol. A* **2000**, *134*, 209.

Manuscript received November 22, 2013; revised manuscript received December 27, 2013; accepted for publication January 7, 2014.